

THEORETICAL STUDY OF SUPERCONDUCTING ANNULAR RING MICROSTRIP ANTENNA WITH SEVERAL DIELECTRIC LAYERS

O. Barkat*

Electronics Department, University of Constantine, Constantine 25000, Algeria

Abstract—An analytical model is presented to investigate the performances of an annular-ring patch etched on a two layered dielectric substrate and is covered by a dielectric superstrate, by using a full-wave spectral domain technique in conjunction with the complex resistive boundary condition. Galerkin's method and Parseval's theorem are used to obtain the resonant frequency and bandwidth. To validate the theoretical results, a study has been performed for an annular-ring patch on a single layer, with air gap, and cover layer. The computed data are found to be in good agreement with results obtained using other methods. Variations of the resonant frequency and bandwidth with the high temperature superconducting (HTS) thin film are also presented. The proposed model is simple, accurate and thus should help a designer for practical applications.

1. INTRODUCTION

Microstrip antennas have been developed over the years and have been widely used in personal mobile communication, wireless local area computer networks, and satellite communication [1, 2]. The rapid advances in the wireless communication industry demand novel antenna designs that could be used in high frequencies and that will allow size reduction. Microstrip antennas have some drawbacks such as narrow bandwidth and relatively low radiation efficiency [3]. In order to further improve the performance of microstrip antennas, it has been proposed to replace the conventional patch structures by high temperature superconducting (HTS) thin film [4–8]. Major

Received 1 February 2012, Accepted 14 March 2012, Scheduled 9 April 2012

* Corresponding author: Ouarda Barkat (barkatwarda@yahoo.fr).

property of superconductor is very low surface resistance compared with normal metals, such as copper, silver, and gold. Using this low surface resistance, superconductors can reduce the insertion loss, and obtain a high efficiency. Owing to the inherent narrow bandwidth of this type of antennas around their operating resonant frequencies, many techniques of bandwidth enhancement have been suggested and designed. Bandwidth of antenna can be increased by using the thick substrate of low dielectric constant or by designing the antenna with several dielectric layers [9–12]. The reason for selection of three dielectric layers is to achieve tunable resonant frequency characteristic by using air gap structure, also for bandwidth enhancement, while the dielectric cover can be used to offer protection against environmental hazards, such as rain, fog, and snow. The benefits of using high temperature superconductors in microstrip antennas can be quite substantial owing to the reduced losses, which translate to an increase in the efficiency of the antenna.

Among the various shapes of patch, the annular ring patch is the ones that has been more extensively studied for a long time by a number of investigators [13–16]. An annular ring microstrip antenna is quite a complicated structure to analyze mathematically. Different models are available to model a microstrip antenna. The transmission-line model and the cavity model in simple computer aided design formulas [17]. However, the accuracy of these approximate models is limited and only suitable for analysing simple, regularly shaped antenna or thin substrates. The full-wave spectral domain technique is extensively used in microstrip analysis and design [18–21]. This method gives better results than approximate techniques. In the current paper, we have developed an analytical model for the analysis of HTS annular-ring patch covered with a dielectric layer and one or two lower substrates which little has been published. Our theoretical study is carried out by using a full-wave spectral domain technique in conjunction with the complex resistive boundary condition.

2. THEORETICAL MODEL

The geometry under consideration is illustrated in Fig. 1. We have an annular ring patch of a and b radius, and thickness t . The substrate is assumed to be made of two layers. The first (second) layer of thickness d_1 (d_2) is characterized by the free-space permeability μ_0 and the complex dielectric permittivity $\bar{\epsilon}_1$ ($\bar{\epsilon}_2$). Above the radiating patch is the superstrate layer of thickness d_3 with permeability μ_0 and a permittivity $\bar{\epsilon}_3$. The ambient medium is air with constitutive parameters μ_0 and ϵ_0 .

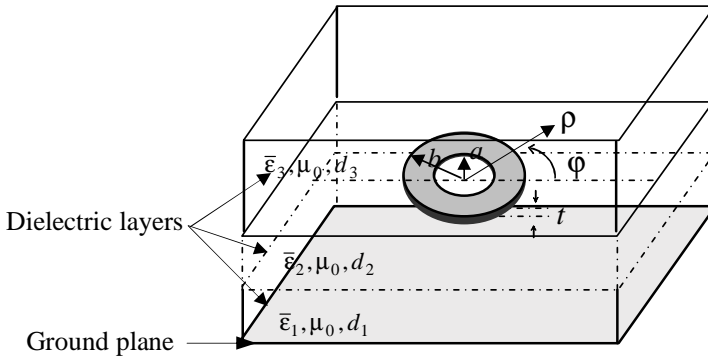


Figure 1. Superconducting annular ring microstrip antenna with several dielectric layers.

In order to solve scattering problems of structure, the full-wave spectral domain technique is a preferred choice for multilayer medium problems. We will suppose that a space time dependence of all the components of the kind $e^{i(\vec{k}\cdot\vec{r}-\omega t)}$. The kernel of electrical field integral equation with Hankel transform domain, is the layered medium Green's function [14]. Using a matrix representation of each layer, it is easily to derive the dyadic Green's function of the problem in a manner very similar to that shown in [15].

$$\bar{G}(k_\rho) = -(\bar{\Gamma}_<)_{12} \cdot [\bar{g}_0 \cdot (\bar{\Gamma}_>)_{12} - (\bar{\Gamma}_>)_{22}] \cdot [\bar{g}_0 \cdot (\bar{\Gamma})_{12} - (\bar{\Gamma})_{22}]^{-1} \quad (1)$$

where

$$\bar{\Gamma}_< = \prod_{j=M}^1 \bar{T}_j, \quad \bar{\Gamma}_> = \prod_{j=N}^{M+1} \bar{T}_j, \quad \text{and } \bar{\Gamma} = \bar{\Gamma}_> \cdot \bar{\Gamma}_< \quad (2)$$

$\prod_{j=M}^1$ and $\prod_{j=N}^{M+1}$ means the product of matrices below and above the annular ring patch.

Here, the expression of the matrices \bar{T}_j for the anisotropy in the dielectrics is given by

$$\bar{T}_j = \begin{bmatrix} \cos(\bar{k}_{jz}d_j) & i \frac{\sin(\bar{k}_{jz}d_j)}{\bar{g}_j(k_\rho)} \\ -i\bar{g}_j(k_\rho) \cdot \sin(\bar{k}_{jz}d_j) & \cos(\bar{k}_{jz}d_j) \end{bmatrix} \quad (3)$$

where

$$\bar{k}_{jz} = \begin{bmatrix} \sqrt{(\varepsilon_{jx}k^2 - \frac{\varepsilon_{jx}}{\varepsilon_{jz}}k_\rho^2)} & 0 \\ 0 & \sqrt{(\varepsilon_{jx}k^2 - k_\rho^2)} \end{bmatrix} \quad (4)$$

and

$$\bar{\mathbf{g}}_j(k_\rho) = \begin{bmatrix} \frac{\omega \varepsilon_{jx} \varepsilon_0}{\sqrt{(\varepsilon_{jx} k^2 - \frac{\varepsilon_{jx}}{\varepsilon_{jz}} k_\rho^2)}} & 0 \\ 0 & \frac{\sqrt{(\varepsilon_{jx} k^2 - k_\rho^2)}}{\omega \mu_0} \end{bmatrix} \quad (5)$$

$k = \omega \sqrt{\mu_0 \varepsilon_0}$: is the free space wavenumber.

After obtaining the dyadic Green's function of multilayered substrate by applying full-wave spectral domain technique, the function is modified by considering surface complex impedance [8]. Assuming the superconducting effects, we need simply to modify (1) by replacing $\bar{G}(k_\rho)$ by $(\bar{G}(k_\rho) - \bar{Z}_S)$, where \bar{Z}_S is the surface impedance of superconducting annular ring patch. When the thickness of the superconducting patch is less than three times the zero-temperature penetration depth (λ_0), \bar{Z}_S can be expressed as follows

$$\bar{Z}_s = \begin{bmatrix} Z_s & 0 \\ 0 & Z_s \end{bmatrix} \quad (6)$$

which

$$Z_s = 1/(\sigma t) \quad (7)$$

where σ is the complex conductivity of the superconducting films. It is determined by using London's equation and the Gorter-Casimir model as [4]

$$\sigma = \sigma_n (T/T_c)^4 - i \left(1 - (T/T_c)^4 \right) / (\omega \mu_0 \lambda_0^2) \quad (8)$$

where T is the temperature, T_c is the transition temperature, σ_n is the normal state conductivity at $T = T_c$, and ω is the angular frequency.

Integral equation method in conjunction with the Galerkin method has been a very popular choice for electromagnetic modeling. The Galerkin method is considered the standard procedure to solve this class of integral equations. It gives the fundamental quantity of interest, namely the electric current distribution on the patch surface from, which all the other required antenna parameters can be obtained. In the literature, basis functions are formed by the set of transverse magnetic (TM) and transverse electric (TE) modes of a cylindrical cavity with magnetic side walls, electric top and bottom walls. Following a mathematical reasoning similar to that shown in [14], the field distributions for the TM_{nm} modes can be shown to be given by

$$\mathbf{E}_{zn}(\rho, \varphi) = \mathbf{E}_n \Psi_n(\beta_{nm} \rho / a) e^{in\varphi} \quad (9)$$

$$\mathbf{H}_{\rho n}(\rho, \varphi) = \left(\frac{n}{\omega \mu \rho} \right) \mathbf{E}_n \Psi_n(\beta_{nm} \rho / a) e^{in\varphi} \quad (10)$$

$$\mathbf{H}_{\varphi n}(\rho, \varphi) = \left(\frac{i \beta_{nm}}{\omega \mu a} \right) \mathbf{E}_n \Psi'_n(\beta_{nm} \rho / a) e^{in\varphi} \quad (11)$$

where

$$\psi(\beta_{nm}\rho/a) = J_n(\beta_{nm}\rho/a)N'_n(\beta_{nm}) - J'_n(\beta_{nm})N_n(\beta_{nm}\rho/a) \quad (12)$$

$$\psi'(\beta_{nm}\rho/a) = J'_n(\beta_{nm}\rho/a)N'_n(\beta_{nm}) - J'_n(\beta_{nm})N'_n(\beta_{nm}\rho/a) \quad (13)$$

J_n and Y_n are the Bessel's and Neuman's functions of order n , respectively.

By using (9)–(11), it is possible to find a complete set of vector basis functions to approximate the current distribution. The current on the HTS annular ring patch corresponding to the field of TM_{nm} modes in a magnetic-wall-cavity is

$$\bar{\mathbf{L}}_{nm}(\rho) = \begin{cases} \begin{bmatrix} \psi'_n(\beta_{nm}\rho/a) \\ \frac{na}{\beta_{nm}\rho}\psi_n(\beta_{nm}\rho/a) \end{bmatrix} & a < \rho < b \\ 0 & \rho > b, \rho < a \end{cases} \quad (14)$$

The current on the HTS annular ring patch corresponding to the field of TE_{nq} mode of the magnetic-wall-cavity modes can be written as

$$\bar{\mathbf{F}}_{nq}(\rho) = \begin{cases} \begin{bmatrix} \frac{na}{\alpha_{nq}\rho}\varphi_n(\alpha_{nq}\rho/a) \\ \varphi'_n(\alpha_{nq}\rho/a) \end{bmatrix} & a < \rho < b \\ 0 & \rho > b, \rho < a \end{cases} \quad (15)$$

where

$$\varphi_n(\alpha_{nq}\rho/a) = J_n(\alpha_{nq}\rho/a)N_n(\alpha_{nq}) - J_n(\alpha_{nq})N_n(\alpha_{nq}\rho/a) \quad (16)$$

$$\varphi'_n(\alpha_{nq}\rho/a) = J'_n(\alpha_{nq}\rho/a)N_n(\alpha_{nq}) - J_n(\alpha_{nq})N'_n(\alpha_{nq}\rho/a) \quad (17)$$

By noting that the superposition of the currents due to TM and TE modes of a magnetic-wall cavity forms a complete set, the current distribution of the n mode of the HTS annular ring patch can be written as

$$K_n(\rho) = \begin{cases} \sum_{m=1}^M a_{nm}\bar{\mathbf{L}}_{nm}(\rho) + \sum_{q=1}^Q b_{nq}\bar{\mathbf{F}}_{nq}(\rho) & a < \rho < b \\ 0 & \rho > b, \rho < a \end{cases} \quad (18)$$

where a_{nm} and b_{nq} are unknown coefficients.

The vector Hankel transforms (VHT) in compact forms as follows [14]

$$K_n(k_\rho) = \int_0^\infty d\rho \cdot \rho \cdot \bar{H}_n(k_\rho\rho) \cdot K_n(\rho) \quad (19)$$

H_n is the kernel of the vector Hankel transform, is given by

$$\bar{H}_n(k_\rho\rho) = \begin{vmatrix} \dot{J}_n(k_\rho\rho) & -inJ_n(k_\rho\rho)/k_\rho \\ inJ_n(k_\rho\rho)/k_\rho & \dot{J}_n(k_\rho\rho) \end{vmatrix} \quad (20)$$

By substituting (18) into (19), vector Hankel transform of the current basis functions can be given by

$$K_n(k_\rho) = \sum_{m=1}^M a_{nm} \int_0^\infty d\rho \cdot \rho \cdot \bar{H}_n(k_\rho \rho) \cdot \bar{L}_{nm}(\rho) + \sum_{q=1}^Q b_{nq} \int_0^\infty d\rho \cdot \rho \cdot \bar{H}_n(k_\rho \rho) \cdot \bar{F}_{nq}(\rho) \quad (21)$$

$\bar{K}_n(k_\rho)$ can be written as

$$\bar{K}_n(k_\rho) = \sum_{m=1}^M a_{nm} \bar{L}_{nm}(k_\rho) + \sum_{q=1}^Q b_{nq} \bar{F}_{nq}(k_\rho) \quad (22)$$

with

$$\bar{L}_{nm}(k_\rho) = \begin{cases} \left[\begin{array}{c} \frac{(\beta_{nm}/a)}{((\beta_{nm}/a)^2 - k_\rho^2)} Y'_{nm}(k_\rho) \\ \frac{na}{(\beta_{nm} k_\rho)} Y_{nm}(k_\rho) \end{array} \right] & a < \rho < b \\ 0 & \rho > b, \rho < a \end{cases} \quad (23)$$

$$\bar{F}_{nq}(k_\rho) = \begin{cases} \left[\begin{array}{c} 0 \\ \frac{k_\rho a}{(k_\rho^2 - (\alpha_{nq}/a)^2)} Z_{nq}(k_\rho) \end{array} \right] & a < \rho < b \\ 0 & \rho > b, \rho < a \end{cases} \quad (24)$$

where

$$Y_{nm}(k_\rho) = \psi_n(\beta_{nm} b/a) J_n(k_\rho b) - \psi_n(\beta_{nm}) J_n(k_\rho a) \quad (25)$$

$$Z_{nq}(k_\rho) = (b/a) \varphi'_n(\alpha_{nq} b/a) J_n(k_\rho b) - \varphi'_n(\alpha_{nq}) J_n(k_\rho a) \quad (26)$$

α_{nq} , β_{nm} are the roots of dual equations $\varphi_n(\alpha_{nq} b/a) = 0$ and $\psi'_n(\beta_{nm} b/a) = 0$

Electric field is enforced to satisfy the impedance boundary condition on the annular ring patch, and the current vanishes off the patch, to give the following set of vector dual integral equations [8]

$$e_n(\rho) = \int_0^\infty dk_\rho k_\rho \bar{H}_n(k_\rho \rho) \cdot (\bar{G}(k_\rho) - \bar{Z}_S) \bar{K}_n(k_\rho) = 0 \quad a < \rho < b \quad (27)$$

$$K_n(\rho) = \int_0^\infty dk_\rho k_\rho \bar{H}_n(k_\rho \rho) \cdot \bar{K}_n(k_\rho) = 0 \quad \rho > b, \rho < a \quad (28)$$

By substituting (22) into (27), we obtain

$$\sum_{m=1}^M a_{nm} \int_0^\infty dk_\rho k_\rho \bar{H}_n(k_\rho, \rho) (\bar{G}(k_\rho) - \bar{Z}_S) \bar{\mathbf{L}}_{nm}(k_\rho) + \sum_{q=1}^Q b_{nq} \int_0^\infty dk_\rho k_\rho \bar{H}_n(k_\rho, \rho) (\bar{G}(k_\rho) - \bar{Z}_S) \bar{\mathbf{F}}_{nq}(k_\rho) = 0 \quad (29)$$

Next, multiplying (29) by $\rho \bar{\mathbf{L}}_{nj}^T(\rho)$ ($j = 1, 2, \dots, M$) and $\rho \bar{\mathbf{F}}_{nk}^T(\rho)$ ($k = 1, 2, \dots, Q$) and integrating from a until to b , and using Parseval's theorem for vector Hankel transform, we will have

$$\sum_{m=1}^M a_{nm} \int_0^\infty dk_\rho k_\rho \bar{\mathbf{L}}_{nj}^T(k_\rho) (\bar{G}(k_\rho) - \bar{Z}_S) \bar{\mathbf{L}}_{nm}(k_\rho) + \sum_{q=1}^Q b_{nq} \int_0^\infty dk_\rho k_\rho \bar{\mathbf{L}}_{nj}^T(k_\rho) (\bar{G}(k_\rho) - \bar{Z}_S) \bar{\mathbf{F}}_{nq}(k_\rho) = 0 \quad j = 1, 2, \dots, M \quad (30)$$

$$\sum_{m=1}^M a_{nm} \int_0^\infty dk_\rho k_\rho \bar{\mathbf{F}}_{nk}^T(k_\rho) (\bar{G}(k_\rho) - \bar{Z}_S) \bar{\mathbf{L}}_{nm}(k_\rho) + \sum_{q=1}^Q b_{nq} \int_0^\infty dk_\rho k_\rho \bar{\mathbf{F}}_{nk}^T(k_\rho) (\bar{G}(k_\rho) - \bar{Z}_S) \bar{\mathbf{F}}_{nq}(k_\rho) = 0 \quad k = 1, 2, \dots, Q \quad (31)$$

Following well known procedures, we obtain a system of $M + Q$ linear algebraic equations for each mode n which may be written in matrix form

$$\sum_{m=1}^M a_{nm} A_{jm}^{LL} + \sum_{q=1}^Q b_{nq} A_{jq}^{LF} = 0 \quad j = 1, 2, \dots, M \quad (32)$$

$$\sum_{m=1}^M a_{nm} A_{km}^{FL} + \sum_{q=1}^Q b_{nq} A_{kq}^{FF} = 0 \quad k = 1, 2, \dots, Q \quad (33)$$

where

$$A_{ij}^{LL} = \int_0^\infty dk_\rho k_\rho \bar{\mathbf{L}}_{ni}^T(k_\rho) \cdot (\bar{G}(k_\rho) - \bar{Z}_S) \cdot \bar{\mathbf{L}}_{nj}(k_\rho) \quad (34)$$

$$A_{ij}^{LF} = A_{ji}^{FL} = \int_0^{\infty} dk_{\rho} k_{\rho} \bar{L}_{ni}^T(k_{\rho}) \cdot (\bar{G}(k_{\rho}) - \bar{Z}_S) \cdot \bar{\mathbf{F}}_{nj}(k_{\rho}) \quad (35)$$

$$A_{ij}^{FF} = \int_0^{\infty} dk_{\rho} k_{\rho} \bar{\mathbf{F}}_{ni}^T(k_{\rho}) \cdot (\bar{G}(k_{\rho}) - \bar{Z}_S) \cdot \bar{\mathbf{F}}_{nj}(k_{\rho}) \quad (36)$$

To enhance the accuracy of the numerical calculation, the integrals of the matrix elements (34)–(36) are evaluated numerically along an integration path deformed above the real axis (in the complex k_{ρ} plane) to avoid the singularities [8]. The resulting system of equations is then solved, for the unknown current modes on the HTS annular ring patch. Nontrivial solutions can exist, if the determinant of (32)–(33) vanishes, that is

$$\det [\bar{A}(f)] = 0 \quad (37)$$

This is the eigenvalue equation for the antenna structure considered here. In general, the roots of this equation are complex numbers indicating, that the structure has complex resonant frequencies ($f = f_r + if_i$). Real parts of the complex resonant frequencies f_r correspond to resonant frequencies, while imaginary parts f_i account for damping due to radiation loss, this can be explained by the fact that the antenna losses energy by radiation. The bandwidth of a microstrip antenna operating around its resonant frequency can be approximately related to its resonant frequency through the well-known formula (BP= $2f_i/f_r$) [22]. Once the problem is solved for the resonant frequency, far field radiations in spherical coordinates are given from

$$\begin{bmatrix} E_{\theta}(\bar{r}) \\ E_{\varphi}(\bar{r}) \end{bmatrix} = \sum_{n=-\infty}^{+\infty} e^{in\varphi} \cdot (-i)^n \cdot e^{ikr} \cdot \bar{T}(\theta) \cdot \bar{V}(k_{\rho}) \cdot (\bar{G}(k_{\rho}) - \bar{Z}_S) \cdot \bar{K}_n(k_{\rho}) \quad (38)$$

where

$$\bar{V}(k_{\rho}) = \begin{bmatrix} 1 & 0 & -\frac{k_{\rho}}{k_z} \\ 0 & 1 & 0 \end{bmatrix} \text{ and } \bar{T}(\theta) = \begin{bmatrix} \cos \theta & 0 & -\sin \theta \\ 0 & 1 & 0 \end{bmatrix}$$

The losses in the antenna comprise dielectric loss P_d the conductor loss P_c , and the radiation loss P_r , the efficiency of the antenna can be defined as

$$\text{efficiency} = P_r / (P_r + P_c + P_d) \quad (39)$$

where

$$P_r = (1/4\eta) \iint |E_{\theta}E_{\theta}^* + E_{\phi}E_{\phi}^*| r^2 \sin \theta d\theta d\phi, \quad P_c = Z_s \iint |H_{\phi}^2 + H_{\rho}^2| dS$$

and

$$P_d = (\omega \varepsilon t g \delta / 2) \iint |E_z|^2 dV$$

3. NUMERICAL RESULTS

3.1. Resonant Frequency and Bandwidth of Perfect Annular-ring Microstrip Single Layer Antenna

As a validation of the different results, we have compared the proposed model with published data. The codes are implemented in FORTRAN programming software. In Table 1, we have calculated the resonant wave number times the inner radius of the ring $k_r a$ ($k_r a = 2\pi f_r a \sqrt{\epsilon_x \epsilon_0 \mu_0}$), as functions of different sizes of the ratio of the substrate thickness d_2 normalized by the inner radius a . The calculated

Table 1. Comparison of the resonant wave number times the inner radius of the ring ($K_r a$) for varying dielectric substrate thickness ($a = 0.71$ cm, $b = 2a$, $\epsilon_{2z} = \epsilon_{2x} = 2.65$, $d_1 = 0$, $d_3 = 0$).

d_2/a	TM ₁₂ Mode			
	Results of [22]		Our results	
	$k_r a$	BP%	$k_r a$	BP%
0.005	$3.26 + i^*$ 0.002	0.12	$3.257 + i^*$ 0.0024	0.15
0.01	$3.24 + i^*$ 0.003	0.19	$3.248 + i^*$ 0.0036	0.22
0.05	$3.13 + i^*$ 0.008	0.51	$3.085 + i^*$ 0.0066	0.43
0.1	$3.01 + i^*$ 0.014	0.93	$2.968 + i^*$ 0.0164	1.11
d_2/a	TM ₁₁ Mode			
	Results of [22]		Our results	
	$k_r a$	BP%	$(k_r a)$	BP%
0.005	$0.67 + i^*$ $1.6 \cdot 10^{-4}$	0.048	$0.676 + i^*$ $1.6 \cdot 10^{-4}$	0.047
0.01	$0.68 + i^*$ $1,7 \cdot 10^{-4}$	0.05	$0.682 + i^*$ $1.8 \cdot 10^{-4}$	0.053
0.05	$0.70 + i^*$ $5.4 \cdot 10^{-4}$	0.15	$0.695 + i^*$ $5.5 \cdot 10^{-4}$	0.16
0.1	$0.71 + i^*$ 0.0012	0.34	$0.705 + i^*$ 0.0012	0.34

percentage bandwidth (BP%) is obtained by using the formula ($\frac{2f_i}{f_r} * 100$). Perfect annular ring patch printed on substrate isotope is excited in the TM_{11} and TM_{12} modes. We found that, for the TM_{11} mode, the imaginary part of $(k_r a)$, which includes the losses by radiation of the structure, is approximately zero. This means that, the TM_{11} mode has weak-radiation. Also, the TM_{12} has relatively high-radiation. It is clear from Table 1 that our results agree very well with results obtained by other authors [22].

As it is seen from Fig. 2, and Fig. 3, the variation of resonant frequency and bandwidth versus substrate thickness d_2 , with three different relative permittivity $\epsilon_{2z} = \epsilon_{2x} = 2.65$, $\epsilon_{2z} = \epsilon_{2x} = 4.6$, and $\epsilon_{2z} = \epsilon_{2x} = 6.4$. Annular-ring microstrip antenna is excited in the TM_{11} and TM_{12} modes. We found that the TM_{11} mode has a very narrow bandwidth, and the resonant frequency increases as d_2 increases.

In addition, we observe that for the TM_{12} mode the resonant frequency decreases as d_2 increases, and has relatively wide bandwidth. Therefore, the TM_{11} mode is good for resonator applications and the TM_{12} mode for antennas. It is for that one does the applications of antenna in the TM_{12} mode, better than in the TM_{11} mode. This is because the equivalent magnetic current densities on the inner and outer radius for the odd radial modes are of opposite polarity.

3.2. Resonant Frequency, Bandwidth and Efficiency of HTS Annular-ring Microstrip Single Layer Antenna

A small microstrip antennas in high frequencies, is sensitive to the conductor resistance of patch, because of its low radiation resistance,

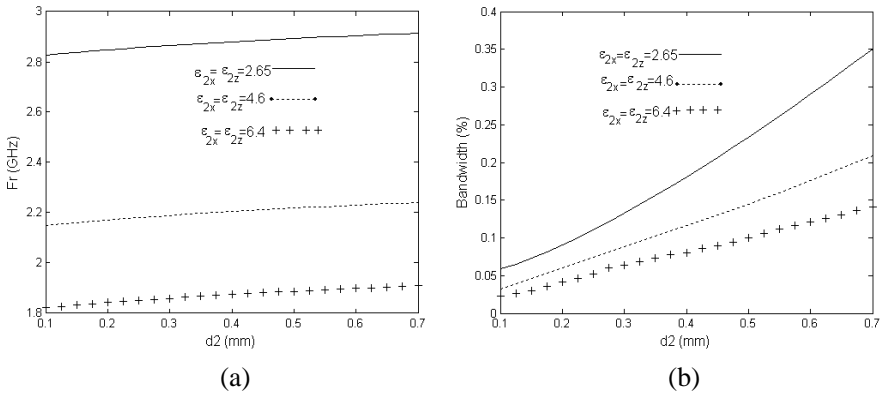


Figure 2. (a) Resonant frequency. (b) Bandwidth versus d_2 of antenna for various isotropic dielectric substrate ($a = 0.71$ cm, $b = 2a$) for mode TM_{11} .

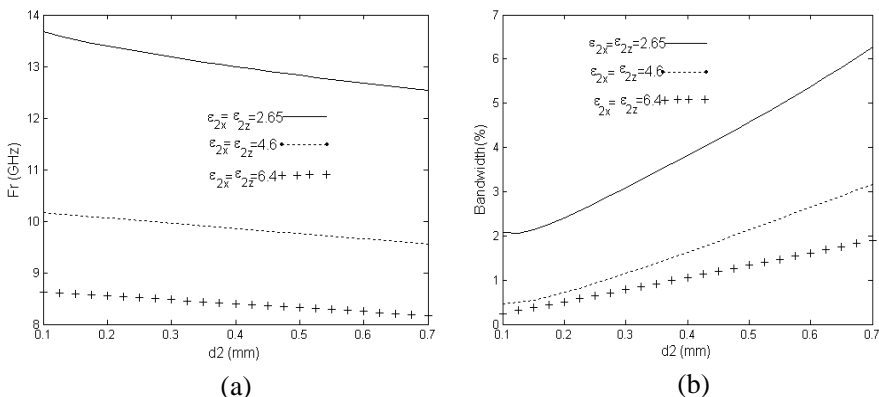


Figure 3. (a) Resonant frequency. (b) Bandwidth versus d_2 of antenna for various isotropic dielectric substrate ($a = 0.71$ cm, $b = 2a$) for TM_{12} mode.

Table 2. Comparison of measured and calculated resonant frequencies of HTS annular ring microstrip antenna ($\sigma_n = 210$ s/mm, $\lambda_0 = 1500$ Å and $T_c = 89$ K, $a = 1.36$ mm, $b = 2.64$ mm, $d_2 = 0.245$ mm, and $t = 1.6$ μm) for TM_{12} mode.

mode	f_{meas} (GHz) [6]	f (GHz) [6]	f (GHz) This model
TM_{11}	5.52	5.46	5.539469975
TM_{21}	10.61	10.65	10.66685079
TM_{31}	15.35	15.44	15.46655754
TM_{12}	21.65	21.70	21.72784215

and the decrease of the radiation efficiency. In order to overcome them, the uses of high temperature superconducting materials for the annular ring patch have been proposed in this work. In order to confirm the computation accuracy, our calculated resonant frequencies are compared with previously published data of Richard et al. [6]. Table 2 summarizes the measured and computed resonant frequencies for different modes as a consequence; good agreement is achieved.

In Fig. 4 we study the influence of the normalized temperature (T/T_c) on the resonant frequency, and the bandwidth of HTS antennas. The annular ring patch has $a = 1.36$ mm, $b = 2.64$ mm, and $t = 1.6$ μm, was fabricated using YBCO high temperature superconducting thin films. The superconducting material characteristics are

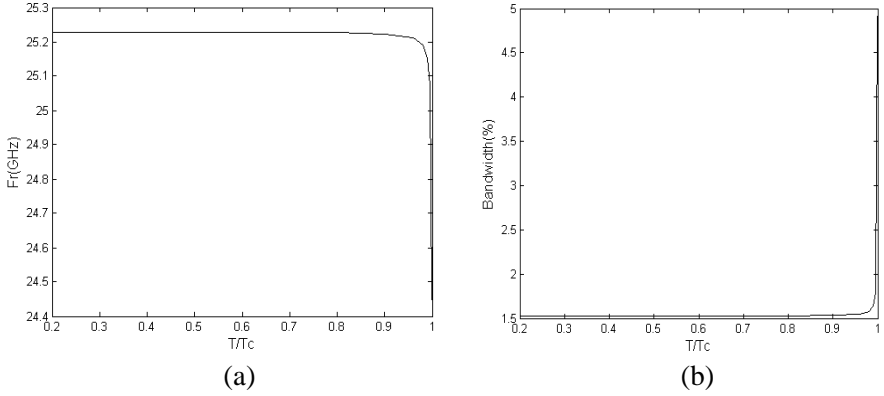


Figure 4. (a) Resonant frequency. (b) Bandwidth versus the normalized temperature T/T_c ($\sigma_n = 210$ s/mm, $\lambda_0 = 1500$ Å and $T_c = 89$ K, $a = 1.36$ mm, $b = 2.64$ mm, $d_2 = 0.245$ mm, $d_1 = 0$ mm, $d_3 = 0$ mm, and $t = 1.6$ μ m).

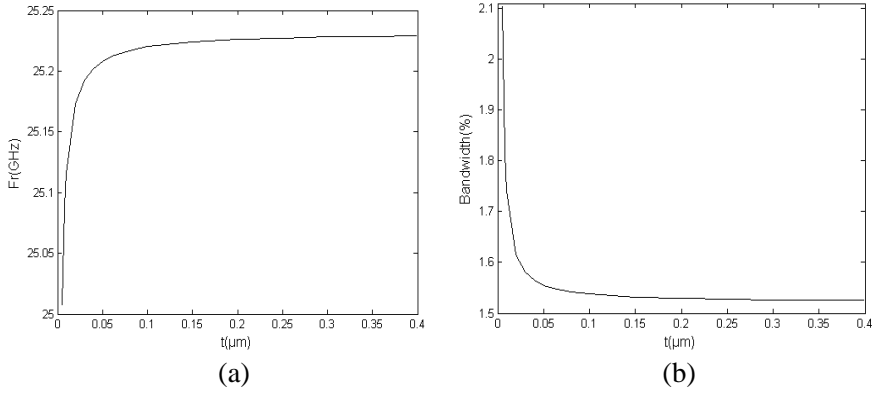


Figure 5. (a) Resonant frequency. (b) Bandwidth versus the thickness t ($\sigma_n = 210$ s/mm, $\lambda_0 = 1500$ Å and $T/T_c = 0.5$, $a = 1.36$ mm, $b = 2.64$ mm, $d = 0.245$ mm).

$\sigma_n = 210$ s/mm, $\lambda_0 = 1500$ Å and $T_c = 89$ K. It is observed that the effect of varying the temperature on the resonant frequency and bandwidth is significant only for temperatures near the critical temperature T_c .

Shown in Fig. 5, is the dependence of resonant frequency and bandwidth on the thickness t of HTS patch. It is observed that,

Table 3. Comparison of calculated efficiencies of HTS annular ring microstrip antenna ($\sigma_n = 10^6$ S/m, $\lambda = 140$ nm, $T_c = 89$ K, $\sigma_C = 40$ S/m, $a = 1.36$ mm, $b = 2.64$ mm, $d_2 = 0.245$ mm and $d_1 = 0$ mm).

Efficiency \ T/T_c	0.112	0.168	0.224	0.337	0.449	0.561	0.6742
YBCO	0.754	0.751	0.747	0.741	0.734	0.729	0.724
copper	0.687	0.684	0.681	0.672	0.664	0.653	0.645

Table 4. Comparison of calculated resonant frequencies of perfect annular ring antenna against the air gap thickness d_1 ($d_2 = 1.59$ mm, $d_3 = 0$ mm, $a = 35$ mm, $b = 2a$, $\epsilon_{2x} = \epsilon_{2z} = 2.32$).

Mode \ d_1	0.5 mm		1 mm	
	f_{meas} (GHz) [11]	f (GHz) This model	f_{meas} (GHz) [11]	f (GHz) This model
TM ₁₁	0.718	0.70695956	0.778	0.763159701
TM ₁₂	3.040	3.09304352	3.240	3.252567562

when the film thickness (t) increases, the resonant frequency increases and bandwidth decrease quickly until the thickness t reaches the value penetration depth (λ_0). After this value, the increase in the frequency of resonance and decrease in bandwidth become less significant.

The efficiencies of the YBCO and copper annular ring microstrip patch antennas are shown in Table 3. It is observed that a maximum improvement of 6.7% in the efficiency at the same temperature.

3.3. Air Gap Tuning Effect on the HTS Annular Ring Microstrip Antenna

Table 4 gives the variations of the theoretical resonance frequency of perfect annular ring antenna against the air gap thickness for TM₁₁ and TM₁₂ modes. we have compared our computed values with measured and theoretical results obtained by [11]. As a consequence, good agreement between theory and experiment is achieved.

Numerical results for the effect of the air separation d_1 on the resonant frequency and bandwidth with various isotropic dielectric substrate of the HTS antenna shown in Fig. 6 and Fig. 7. The superconducting patch of radius $a = 35$.mm and $b = 2a$, is fabricated with an YBCO thin film and the substrate thickness is $d_2 = 1.59$ mm. It is observed that when the air separation grows, the resonant frequency increases rapidly until achieving a maximum operating frequency at a definite air separation d_{1max} . Also the effect of the

air gap is more pronounced for small values of d_1 for TM_{ll} and TM_{I2} . Note that the bandwidth increases monotonically with increasing air separation for TM_{ll} and TM_{I2} modes.

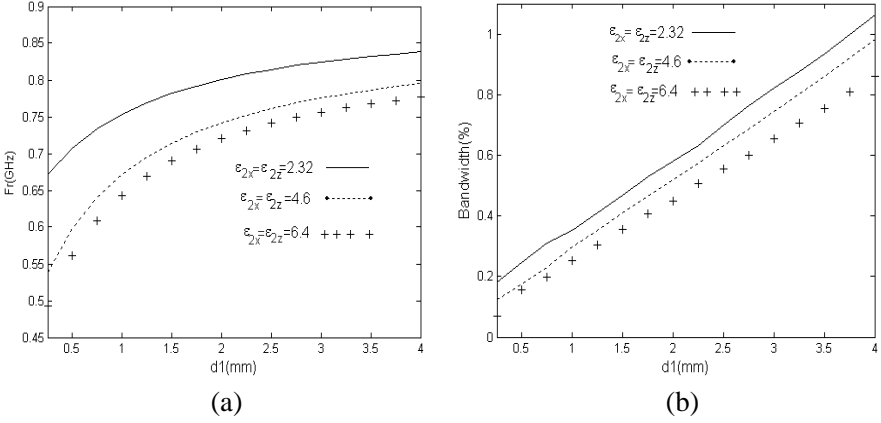


Figure 6. (a) Resonant frequency. (b) Bandwidth versus the air separation d_1 of HTS antenna for various isotropic dielectric substrate ($d_2 = 1.59$ mm, $d_3 = 0$ mm, $a = 35$ mm, $b = 2a$, $\sigma_n = 210$ s/mm, $\lambda_0 = 1500$ Å and $T/T_c = 0.5$, $t = 1.6$ μm) for TM_{11} mode.

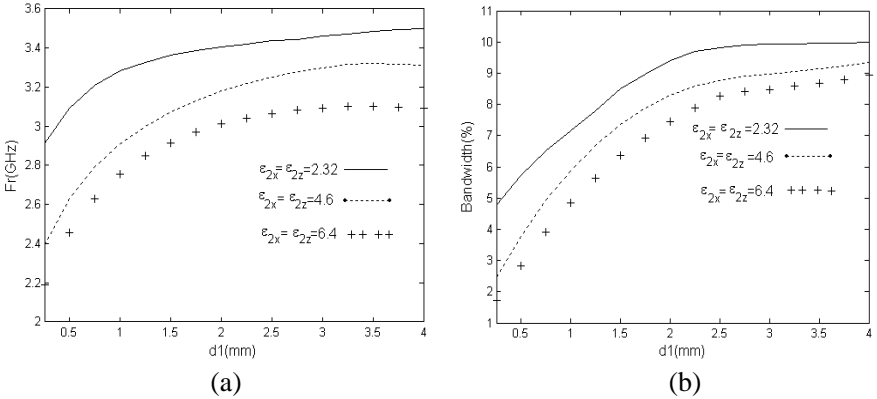


Figure 7. (a) Resonant frequency. (b) Bandwidth versus the air separation d_1 of HTS antenna for various isotropic dielectric substrate ($d_2 = 1.59$ mm, $d_3 = 0$ mm, $a = 35$ mm, $b = 2a$, $\sigma_n = 210$ s/mm, $\lambda_0 = 1500$ Å and $T/T_c = 0.5$, $t = 1.6$ μm) for TM_{12} mode.

3.4. HTS Annular Ring Microstrip with Several Dielectric Layers

The normalized resonant frequency versus the ratio of superstrate thickness d_3 to the substrate thickness d_2 , is presented in Fig. 8(a), the normalization is with respect to f_0 of the magnetic-wall cavity. It is seen that the resonant frequency decreases monotonically with increasing superstrate thickness, the rate of decrease being greater for high permittivity loading. In Fig. 8(b), the normalized bandwidth for different dielectric constants of the superstrate is shown. The numerical results show that for low dielectric constants and small thicknesses ($d_3 < d_2$) of loading dielectric sheets, the bandwidth is almost constant. For large thicknesses ($d_3 > d_2$), the bandwidth increases slowly.

The present model also can be used to investigate the performance of HTS annular-ring patch etched on a two layered dielectric substrate

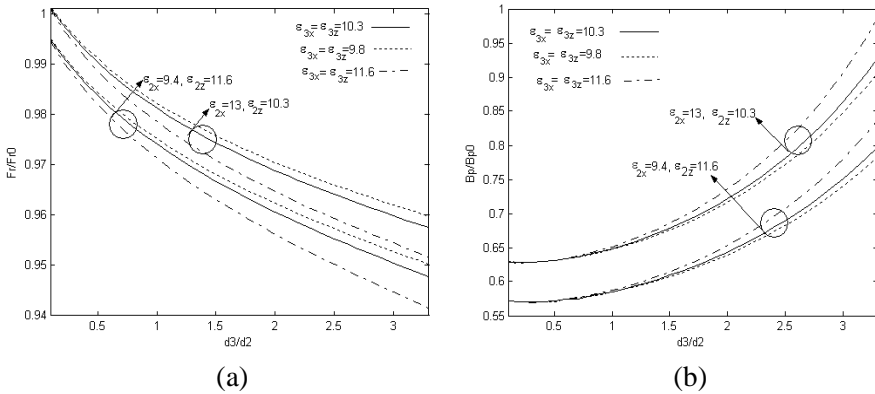


Figure 8. (a) Resonant frequency normalized. (b) Bandwidth normalized versus (d_3/d_2) of HTS antenna ($d_1 = 0$ cm, $d_2 = 0.159$ cm, $a = 3$ cm, $b = 2a$, $\sigma_n = 210$ s/mm, $\lambda_0 = 1500$ Å and $T/T_c = 0.5$, $t = 1.6$ μm) for TM_{12} mode.

Table 5. The resonant frequency versus (b/a) of HTS antenna covered by a dielectric superstrate and with air gap ($\sigma_n = 210$ s/mm, $\lambda_0 = 1500$ Å and $T/T_c = 0.5$, $t = 1.6$ μm, $\epsilon_{1x} = \epsilon_{1z} = 1$, $d_1 = 0.635$ mm, $\epsilon_{2x} = \epsilon_{2z} = 2.32$, $d_2 = 0.635$ mm; $\epsilon_{3x} = \epsilon_{3z} = 6.4$, $d_3 = 0.635$ mm).

b/a	1.5	1.75	2	2.25	2.50
fr (GHz)	8.076856	5.861648	4.522729	3.824951	3.498405

and is covered by a dielectric superstrate. Table 5 depicts the influence of the ratio of outer radius to the inner radius on the resonant frequency of structure. As the aspect ratio increases, the resonant frequency decreases.

4. CONCLUSIONS

Theoretical results for the resonant frequency and bandwidth have been presented for various an annular-ring microstrip antennas configurations. A spectral domain approach has been used for the numerical calculation. The computed data are found to be in good agreement with results obtained using other methods. To include the effect of the superconductivity of the microstrip patch in the spectral domain analysis, the surface complex impedance has been considered. The findings of this work show that in the TM_{11} mode, the annular ring has a very narrow bandwidth. However, in the higher-order TM_{12} mode the annular ring antenna has been shown to have a significantly higher bandwidth. Numerical results for the effect of the temperature and thickness of HTS thin film on the resonant frequency and bandwidth have been presented. In the case of an annular ring microstrip antenna with superstrate, it is found that resonant frequency decreases with increasing superstrate thickness and bandwidth increases for especially increasing superstrate dielectric constant values. Other results also have indicated that the resonant frequencies can be tuned and the bandwidths widened by using structure having an air gap.

REFERENCES

1. Montero-de-Paz, J., E. Ugarte-Muñoz, F. J. Herraiz-Martínez, and V. Gonzalez-Posadas, "Multifrequency self-diplexed single patch antennas loaded with split ring resonators," *Progress In Electromagnetics Research*, Vol. 113, 47–66, 2011.
2. Yang, M. G., X. Xing, A. Daigle, O. Obi, M. Liu, J. Lou, S. Stoute, K. Naishadham, and N. X. Sun, "Planar annular ring antennas with multilayer self-biased nico-ferrite films loading," *IEEE Transactions on Antennas and Propagation*, Vol. 58, No. 3, 648–655, 2010.
3. Balanis, E. C., *Antenna Theory, Analysis and Design*, 2nd Edition, John Wiley & Sons, New York, 1997.

4. Hansen, C. R., *Electrically Small, Superdirective, and Superconducting Antennas*, John Wiley & Sons, Inc, Hoboken, New Jersey, 2006.
5. Wu, C.-J. and Y.-L. Chen, "Microwave properties of a high-temperature superconductor and ferromagnetic bilayer structure," *Progress In Electromagnetics Research*, Vol. 111, 433–445, 2011.
6. Richard, M. A., K. B. Bhasin, and P. C. Claspy, "Performance of a K-band superconducting annular ring antenna," *Microwave and Optical Technology Letters*, Vol. 5, No. 6, 257–259, Jun. 1992.
7. Liu, F. S., X. W. Shi, and S. D. Liu, "Study on the impedance-matching technique for high-temperature superconducting microstrip antennas," *Progress In Electromagnetics Research*, Vol. 77, 281–284, 2007.
8. Barkat, O. and A. Benghalia, "Radiation and resonant frequency of superconducting annular ring microstrip antenna on uniaxial anisotropic media," *Int. J. Infrared Millim. Waves*, Vol. 30, 1053–1066, Jun. 2009.
9. Losada, V., R. R. Boix, and M. Horno, "Resonant modes of circular microstrip patches in multilayered substrates," *IEEE Transactions on Microwave Theory and Techniques*, Vol. 47, 488–498, 2000.
10. Fan, Z. and K. F. Lee, "Input impedance of annular-ring microstrip antennas with a dielectric cover," *IEEE Transactions on Antennas and Propagation*, Vol. 40, No. 8, 992–995, 1992.
11. Dahele, S. J. and K. F. Lee, "Theory and experiments on microstrip antennas with airgaps," *Proc. IEE*, Vol. 132, 455–460, Dec. 1985.
12. Jamlos, F. M., T. A. Rahman, M. R. Kamarudin, M. T. Ali, M. N. M. Tan, and P. Saad, "The gain effects of air gap quadratic aperture-coupled microstrip antenna array," *PIERS Proceedings*, 462–465, Cambridge, USA, Jul. 2010.
13. Gürel, S. Ç. and E. Yazgan, "Modified cavity model to determine resonant frequency of tunable microstrip ring antennas," *Taylor and Francis, Electromagnetic*, Vol. 19, 443–455, 1999.
14. Ali, S. M., W. C. Chew, and J. A. Kong, "Vector Hankel transform analysis of annular ring microstrip antenna," *IEEE Transactions on Antennas and Propagation*, Vol. 30, No. 4, 637–644, Jul. 1982.
15. Barkat, W. and A. Benghalia, "Annular ring microstrip antenna in multilayered media containing uniaxial dielectrics," *First Int. Symp. on Control, Commun. and Signal Processing*, 327–330, 2004.

16. Liu, H. and X. F. Hu, "Input impedance analysis of a microstrip annular-ring antenna with a thick substrate," *Progress In Electromagnetics Research*, Vol. 12, 177–204, 1996.
17. Tagle, J. G. and C. G. Christodoulou, "Extended cavity model analysis of stacked microstrip ring antennas," *IEEE Transactions on Antennas and Propagation*, Vol. 45, No. 11, 1626–1635, 1997.
18. Motevasselian, A., "Spectral domain analysis of resonant characteristics and radiation patterns of a circular disc and an annular ring microstrip antenna uniaxial substrate," *Progress In Electromagnetics Research M*, Vol. 21, 237–251, 2011.
19. Pergol, M. and W. Zieniutycz, "Rectangular microstrip resonator illuminated by normal-incident plane wave," *Progress In Electromagnetics Research*, Vol. 120, 83–97, 2011.
20. Gürel, S. Ç. and E. Yazgan, "Resonant frequency analysis of annular ring microstrip patch on uniaxial medium via Hankel transform domain immittance approach," *Progress In Electromagnetics Research M*, Vol. 11, 37–52, 2010.
21. Firouzeh, Z. H., G. A. E. Vandenbosch, R. Moini, S. H. H. Sadeghi, and R. Faraji-Dana, "Efficient evaluation of Green's functions for lossy half-space problems," *Progress In Electromagnetics Research*, Vol. 109, 139–157, 2010.
22. Chew, W. C., "A broad band annular ring microstrip antenna," *IEEE Transactions on Antennas and Propagation*, Vol. 30, 918–922, 1982.